Highly Luminescent NIR-to-Visible Upconversion Thin Films and Monoliths Requiring No High-Temperature Treatment

Cuikun Lin, Mary T. Berry, Robert Anderson,[†] Steve Smith,[†] and P. Stanley May*

Department of Chemistry, University of South Dakota, 414 East Clark Street, Vermillion, South Dakota 57069. [†]Nanoscience and Nanoengineering, South Dakota School of Mines and Technology, Rapid City, South Dakota 57701

A method is described for producing highly luminescent composite NIR-to-visible upconversion thin films, made from β-NaYF$_4$:3%Er,17%Yb nanocrystals in a polymethyl methacrylate (PMMA) matrix, which require no postdeposition heat treatment. Nanocrystals are synthesized via a single-phase, high-boiling-point solvent method, which requires neither metal-trifluoroacetate precursors nor the use of autoclaves. Highly luminescent films are produced that can be varied in thickness down to dimensions approaching those of the nanocrystals themselves. The physical properties of the films are characterized by AFM and TEM, whereas the spectroscopic properties are characterized by NIR-to-visible confocal microscopy and by the time-dependence of upconversion luminescence following pulsed NIR excitation. It is shown that dispersal of β-NaYF$_4$:3%Er,17%Yb nanocrystals in PMMA has no adverse effect on the intrinsic quantum efficiency of upconversion. By focusing the NIR pump beam (980 nm, cw) in the film, linear intensity response and constant color balance are achieved at pump powers down to 40 μW. It is also demonstrated that the thin-film method can be modified to produce large NIR-to-visible upconversion monoliths of high optical quality. This study supports an earlier assertion that the upconversion properties of β-NaYF$_4$:Er,Yb nanocrystals approach those of the bulk material when nanocrystal size is greater than $\sim$70 nm.

Introduction

Upconversion (UC) phosphors have numerous potential applications in science and technology. There is particular interest in upconversion phosphors that can efficiently convert near-infrared (NIR) excitation from inexpensive diode lasers into visible luminescence.[1] Moreover, the availability of UC phosphors in nanocrystalline form greatly increases the breadth of potential applications for these materials in science and technology. Nanocrystalline NIR-to-visible upconverters, for example, have significant potential in areas such as biological labels,[2–5] because NIR excitation penetrates deeply into biological tissue and generates virtually no unwanted fluorescence background signal. NIR-to-visible UC nanocrystals have been proposed for photodynamic therapy applications,[6] for which the high penetration depth of NIR light in biological tissue is again an advantage. In addition, NIR-to-visible UC nanocrystals show considerable promise for applications in the development of 3D luminescent displays that use NIR lasers to generate the 3D image.[7–9]

Some of the more promising technological applications of UC luminescence require thin-films of the UC materials. The use of UC thin-films has been proposed in designs for multilayer optical storage disks,[10] photoluminescent screens for optically written displays,[11] and photovoltaic cells that capture sub-bandgap solar radiation.[12,13] By far the most commonly reported upconverting thin films are produced by sol−gel techniques and are activated by rare-earth (RE) oxides[14] or fluorides.[15,16] However, sol−gel-produced upconversion films typically require postdeposition heat treatment to reduce the concentration of quenching −OH oscillators and achieve acceptable luminescence efficiencies. Heat treatment may be undesirable

*Corresponding author. E-mail: smay@usd.edu.
(1) Suyver, J. F.; Aebischer, A.; Biner, D.; Gerner, P.; Grimm, J.; Heer, S.; Krämer, K. W.; Reinhard, C.; Güdel, H. U. *Opt. Mater.* **2005,** *27*, 1111–1130.
(2) Chen, Z.; Chen, H.; Hu, H.; Yu, M.; Li, F.; Zhang, Q.; Zhou, Z.; Yi, T.; Huang, C. *J. Am. Chem. Soc.* **2008,** *130*, 3023–3029.
(3) Lim, S. F.; Riehn, R.; Ryu, W. S.; Khanarian, N.; Tung, C.-k.; Tank, D.; Austin, R. H. *Nano Lett.* **2006,** *6*, 169–174.
(4) Salthouse, C.; Hilderbrand, S.; Weissleder, R.; Mahmood, U. *Opt. Express* **2008,** *16*, 21731–21737.
(5) Zhang, P.; Rogelj, S.; Nguyen, K.; Wheeler, D. *J. Am. Chem. Soc.* **2006,** *128*, 12410–12411.
(6) Zhang, P.; Steelant, W.; Kumar, M.; Scholfield, M. *J. Am. Chem. Soc.* **2007,** *129*, 4526–4527.

(7) Hinklin, T. R.; Rand, S. C.; Laine, R. M. *Adv. Mater.* **2008,** *20*, 1270–1273.
(8) Downing, E.; Hesselink, L.; Ralston, J.; Macfarlane, R. *Science* **1996,** *273*, 1185–1189.
(9) Liu, X.; Dong, G.; Qiao, Y.; Qiu, J. *Appl. Opt.* **2008,** *47*, 6416–6421.
(10) Ho, H. P.; Wong, W. W.; Wu, S. Y. *Opt. Eng.* **2003,** *42*, 2349–2353.
(11) Wang, Q. H.; Bass, M. *Electron. Lett.* **2004,** *40*, 987–988.
(12) Shalav, A.; Richards, B. S.; Trupke, T.; Krämer, K. W.; Güdel, H. U. *Appl. Phys. Lett.* **2005,** *86*, 013505–3.
(13) Richards, B. S.; Shalav, A. *Synth. Met.* **2005,** *154*, 61–64.
(14) Que, W.; Zhou, Y.; Lam, Y. L.; Pita, K.; Chan, Y. C.; Kam, C. H. *Appl. Phys. A: Mater. Sci. Process.* **2001,** *73*, 209–213.
(15) Sivakumar, S.; vanVeggel, F. C. J. M.; Raudsepp, M. *J. Am. Chem. Soc.* **2005,** *127*, 12464–12465.
(16) Sivakumar, S.; vanVeggel, F. C. J. M.; May, P. S. *J. Am. Chem. Soc.* **2007,** *129*, 620–625.

Article

Chem. Mater., Vol. 21, No. 14, 2009 3407

for a variety of reasons, including the fact that it can induce reactions between the gel and the phosphors, making the luminescence properties of the film unpredictable. Also, it excludes applications on heat-sensitive substrates. Pulsed laser deposition (PLD) has also been used to successfully produce NIR-to-visible and NIR-to-UV UC thin films,[17,18] and although PLD does not require postdeposition heat treatment, it is a relatively expensive and complex technique.

In the limit of high excitation flux, the intrinsic quantum efficiencies of UC phosphors can be quite high. β-NaYF$_4$:Er,Yb is the most efficient NIR-to-visible UC material described to date.[1,19] Suyver et al. estimate that in the high-power excitation region, ~50% of the NIR photons absorbed by NaYF$_4$:2%Er^{3+},18%Yb^{3+} contribute directly to mechanisms leading to the emission of visible light.[19] Recently, the development of synthetic methods for producing solvent-dispersible nanocrystals of phase-pure β-NaYF$_4$:Ln,Yb (Ln = Er^{3+}, Tm^{3+})[20−30] has stimulated a noticeable increase in published upconversion studies.

In this article, a method is described for producing composite NIR-to-visible upconverting thin films made from β-NaYF$_4$:3%Er,17%Yb nanocrystals in a polymethyl methacrylate (PMMA) matrix. β-NaYF$_4$: 3%Er,17%Yb nanoparticles were prepared by a facile, single-phase, high-boiling-point solvent method developed in our lab that requires neither metal trifluoroacetate precursors nor extended reaction times in an autoclave. Trifluoroacetic acid and its derivatives must be handled with some care, and the decomposition of metal trifluoroacetate can produce toxic gases.[31] The current method is quite safe and uses NaF and lanthanide acetates as precursors, and a mixture of oleic acid (OA) and 1-octadecene as the solvent. Although similar in some aspects to other reported methods that use NaF as the fluoride source,[27,28,30] the current procedure is carried out at atmospheric pressure in a single-phase reaction mixture. It is demonstrated that highly luminescent films are produced that can be varied in thickness down to dimensions approaching those of the nanocrystals themselves. Dispersal of the nanocrystals in PMMA has no adverse effect on the intrinsic quantum efficiency of upconversion, and no post-deposition heat treatment of thin films is required. The luminescence properties of the film are predictable and controllable, because they are determined entirely by the intrinsic luminescence properties of the nanocrystalline activators. Also, by focusing the NIR pump beam (980 nm) in the film, linear color response can be achieved at absolute pump powers below 40 μW (cw). It is also demonstrated that the thin film method can be modified to produce large NIR-to-visible UC monoliths of high optical quality.

Experimental Section

Materials. Sodium fluoride (NaF), and acetic acid (CH$_3$COOH) were obtained from Fisher Scientific. Yttrium oxide (Y$_2$O$_3$, 99.9%), ytterbium oxide (Yb$_2$O$_3$, 99.9%) and erbium oxide (Er$_2$O$_3$, 99.9%) were purchased from American Potash & Chemical Co. Sodium acetate (CH$_3$COONa), 2,2'-azobis(2-methylpropionitrile) (AIBN), methyl methacrylate (MMA), oleic acid, and 1-octadecene were obtained from Aldrich. Poly(methyl methacrylate) (PMMA, 350000 g/mol) was purchased from Alfa. Rare earth acetates were prepared by dissolving the corresponding rare-earth oxides into 50:50 (v/v) water:glacial acetic acid and then evaporating the solvent.

Synthesis of β-NaYF$_4$:3%Er,17%Yb Nanocrystals. To prepare β-NaYF$_4$:3%Er,17%Yb nanocrystals, 0.4 mmol Y(CH$_3$COO)$_3$, 0.085 mmol Yb(CH$_3$COO)$_3$, and 0.015 mmol Er(CH$_3$COO)$_3$ was dissolved in 6 mL of oleic acid. The mixture was held at 100 °C under a vacuum for 60 min to purge oxygen and water. The fluoride-containing solution was prepared by dissolving 1 mmol of CH$_3$COONa and 2 mmol of NaF in 2 mL of oleic acid and 10 mL of 1-octadecene. The mixture was kept at 100 °C under a vacuum for 30 min, with periodic purging with Ar. The fluoride solution was then heated under Ar to 320 °C within 10−15 min and maintained at this temperature. This solution became clear and homogeneous at temperatures above 240 °C. The lanthanide solution was then injected into the fluoride solution within 1 min. The homogeneous, single-phase reaction mixture was maintained at 320 °C for 30 min under Ar and then allowed to cool to room temperature. The nanoparticles were then precipitated by the addition of ~100 mL of acetone and isolated by centrifugation at 5000 rpm. The samples were then washed with acetone at least three times. The product, as isolated, was ~20 wt % nanocrystals; the remainder of the mass was oleic acid. The yield of this synthesis was ~73%. The reported concentration of Er^{3+} and Yb^{3+} in the nanocrystals is nominal, based on the composition of the starting materials. The resulting nanoparticles were easily dispersed in nonpolar solvents such as hexane, toluene, and chloroform. The synthesis of β-NaYF$_4$ was confirmed by powder X-ray diffraction. This procedure resulted in nanocrystals of ~72 nm in diameter across the hexagonal face (as determined by TEM). Larger crystals were obtained by increasing the reaction time following the addition of the lanthanide precursors to the fluoride-containing solution.

Preparation of Upconversion Thin Films. 100 mg NaYF$_4$:3% Er,17%Yb nanoparticles and 100 mg PMMA (average weight = 350000 g/mol) were dissolved in 12 mL of chloroform (CHCl$_3$) with vigorous stirring. The β-NaYF$_4$:3%Er,17%Yb-PMMA thin film was prepared by spin-coating this solution on a glass slide (3500 rpm).

Upconverting Thin-Film Characterization. AFM images were measured using a Nano-R2 from Pacific Nanotechnology in

(17) Qin, G.; Qin, W.; Wu, C.; Huang, S.; Zhang, J.; Lu, S.; Zhao, D.; Liu, H. *J. Appl. Phys.* **2003**, *93*, 4328–4330.
(18) Bubb, D. M.; Cohen, D.; Qadri, S. B. *Appl. Phys. Lett.* **2005**, *87*, 131909–3.
(19) Suyver, J. F.; Grimm, J.; Krämer, K. W.; Güdel, H. U. *J. Lumin.* **2005**, *114*, 53–59.
(20) Liang, X.; Wang, X.; Zhuang, J.; Peng, Q.; Li, Y. *Adv. Funct. Mater.* **2007**, *17*, 2757.
(21) Sun, Y.; Chen, Y.; Tian, L.; Yu, Y.; Kong, X.; Zhao, J.; Zhang, H. *Nanotechnology* **2007**, *18*, 275609.
(22) Ghosh, P.; Patra, A. *J. Phys. Chem. C* **2008**, *112*, 3223–3231.
(23) Yi, G. S.; Chow, G. M. *Chem. Mater.* **2007**, *19*, 341–343.
(24) Mai, H. X.; Zhang, Y. W.; Sun, L. D.; Yan, C. H. *J. Phys. Chem. C* **2007**, *111*, 13721–13729.
(25) Mai, H. X.; Zhang, Y. W.; Si, R.; Yan, Z. G.; Sun, L. D.; You, L. P.; Yan, C. H. *J. Am. Chem. Soc.* **2006**, *128*, 6426–6436.
(26) Wang, L.; Li, Y. *Nano Lett.* **2006**, *6*, 1645–1649.
(27) Wang, L.; Li, Y. *Chem. Mater.* **2007**, *19*, 727–734.
(28) Wei, Y.; Lu, F.; Zhang, X.; Chen, D. *Chem. Mater.* **2006**, *18*, 5733–5737.
(29) Yi, G. S.; Chow, G. M. *Adv. Funct. Mater* **2006**, *16*, 2324–9.
(30) Li, C.; Quan, Z.; Yang, J.; Yang, P.; Lin, J. *Inorg. Chem.* **2007**, *46*, 6329–6337.
(31) Boyer, J. C.; Vetrone, F.; Cuccia, L. A.; Capobianco, J. A. *J. Am. Chem. Soc.* **2006**, *128*, 7444–7445.

close-contact mode. Film thicknesses were also determined using AFM.

TEM images of thin-films spin coated onto copper TEM supports were acquired with a Hitachi H-7000 FA TEM operated at 125 KV using a 14-bit Olympus side-mounted digital camera.

Preparation of Upconversion Monoliths. Highly transparent β-NaYF$_4$: 3%Er, 17%Yb-PMMA monoliths were synthesized on the basis of the in situ polymerization of MMA. One-hundred milligrams of β-NaYF$_4$:3%Er,17%Yb nanocrystals and 8 mg of AIBN were dissolved in 15 mL of MMA solution with vigorous stirring in a glass vial. The solution was then stirred in an 80 °C water bath for 30 min and then, after the stir bar was removed, placed in oven at 52 °C for 12 h. The resulting monolith was then allowed to slowly cool to room temperature and subsequently removed from the vial by breaking the glass.

Confocal Upconversion Luminescence Microscopy. Confocal upconversion luminescence microscopy measurements were performed at the Center for Nanoscale Materials (CNM) at Argonne National Laboratory. The experimental apparatus consisted of a mode-locked Ti:sapphire laser (Mira 900, Coherent) producing 120 fs pulses at a repetition rate of 76 MHz and an excitation wavelength of 980 nm. The Ti:sapphire laser was pumped with the 532 nm output of a Nd:Vanadate laser (Verdi V10, Coherent). The laser beam was linearly polarized and directed into a confocal microscope equipped with a 0.8 numerical aperture objective. An average excitation power of ~240 μW, corresponding to a power flux of ~75 μW/μm^2, was used to obtain the confocal image shown herein. Upconversion signal was detected in photon counting mode, using an avalanche photodiode (Micro Photon Devices, PDM series). The upconversion emission spectra obtained from various points on the confocal scan were obtained by feeding the luminescence collected by the microscope into a 1/4 m spectrograph (Andor Model SR 303i) equipped with a CCD camera (Andor DU420A CCD).

Upconversion Luminescence Kinetics. Samples were excited with pulsed 984 nm light from an optical parametric oscillator (Opotek Opolette). Excitation powers were ~400 μJ/pulse (fwhm $\approx$ 4 ns), and the excitation beam was focused to ~1 mm in diameter. Upconversion emission was collected and focused with an F-matching lens into a 1/3 m monochromator (Jobin-Yvon, Triax 320) equipped with a red-sensitive photomultiplier tube (Hamamatsu, R928). Luminescence signal was detected using time-resolved photon counting by feeding the detector output directly into a multichannel scalar (Stanford Research Systems, SR 430). Emission was monitored at 539 and 654 nm for the green and red upconversion, respectively. Curve fitting was accomplished using Igor Pro (v. 6.01)

Results and Discussion

Nanocrystal Synthesis. Figure 1 shows the powder X-ray diffraction (XRD) patterns of NaYF$_4$:3%Er, 17%Yb nanoparticles as a function of reaction temperature from 240 to 320 °C. The corresponding standard cards ICCD 77−2042 (α, cubic phase) and ICCD 16−0334 (β, hexagonal phase) are also shown in Figure 1. At 240 °C, the XRD can be indexed to the pure cubic phase (α) ICCD 77−2042. At 300 °C, the XRD shows features of both the cubic phase and hexagonal phase. At 320 °C, the XRD pattern of the sample can be indexed to pure hexagonal phase (β) ICCD 16−0334. For UC
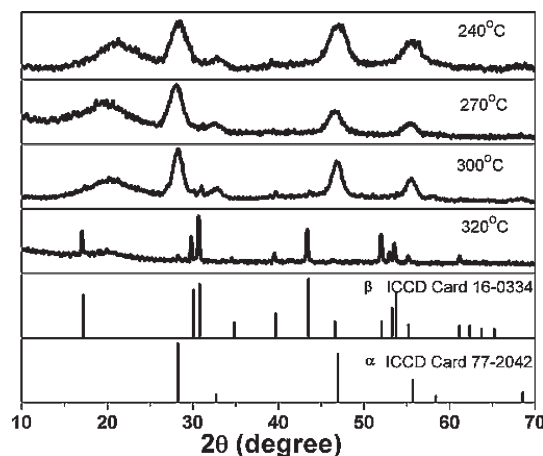
Figure 1. Powder X-ray diffraction (XRD) patterns of NaYF$_4$:3% Er,17%Yb nanocrystals synthesized as described herein. The pure hexagonal (β) phase is produced at a reaction temperature of 320 °C. The standard cards ICCD 77−2042 (α, cubic phase) and ICCD 16−0334 (β, hexagonal phase) are shown for comparison.

applications, the hexagonal (β) phase is strongly preferred to the cubic (α). Krämer, et al. have demonstrated for NaYF$_4$:Er,Yb powder samples that green upconversion for the β phase is 10× more efficient compared to the α phase, while red upconversion is 4.4× as efficient.[32]

Hexagonal plates of the β-phase nanocrystals are produced by the method described herein. The size of the plates is determined by the reaction time at 320 °C. The smallest β-phase nanocrystals that can be practically synthesized by this method are ~50 nm across the hexagonal face (using a 20 min reaction time). The ~72 nm crystals used in the thin films and monoliths described herein are produced by a 30 min reaction time, whereas ~100 nm crystals are produced at 40 min. As reaction times are extended past 1 h, the reaction mixture becomes turbid as the nanocrytalline dispersions become unstable.

As outlined in the Introduction, the synthetic method described herein for producing phase-pure β-NaYF$_4$ nanocrystals is safe, quick, and very robust. We are aware of only one other procedure, that of Wei, et al., that uses NaF as the fluoride-containing precursor and does not require extended reaction times in an autoclave.[28] The advantage of the current procedure is that the reaction is carried out in a single-phase at a higher temperature, which eliminates the problems of contamination from NaF and α-NaYF$_4$ in the final product.

Characterization of Upconversion Thin Films. The basic mechanism for NIR-to-visible upconversion in β-NaYF$_4$: Er,Yb is well-known,[1,33−35] and is schematically illustrated in Figure 2. NIR excitation light is absorbed by Yb^{3+} sensitizers via the $^2F_{7/2} \rightarrow {}^2F_{5/2}$ transition. Electronic excitation energy is then nonradiatively transferred from Yb^{3+}($^2F_{5/2}$) to Er^{3+}($^4I_{15/2}$), resulting in an excited
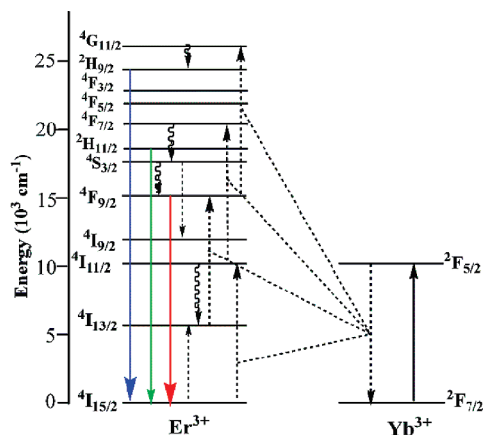
(32) Krämer, K. W.; Biner, D.; Frei, G.; Güdel, H. U.; Hehlen, M. P.; Luthi, S. R. *Chem. Mater.* **2004**, *16*, 1244–1251.
(33) Auzel, F. *Chem. Rev.* **2004**, *104*, 139–174.
(34) Heer, S.; Kompe, K.; Güdel, H. U.; Haase, M. *Adv. Mater.* **2004**, *16*, 2102–2105.
(35) Suyver, J. F.; Grimm, J.; van Veen, M. K.; Biner, D.; Krämer, K. W.; Güdel, H. U. *J. Lumin.* **2006**, *117*, 1–12.

Figure 2. Energy level diagram illustrating the mechanism of upconversion of NIR excitation to blue, green, and red emission in NaYF$_4$: Er, Yb.

Er^{3+} ($^4I_{11/2}$) ion and a ground-state Yb^{3+}($^2F_{7/2}$) ion. This energy-transfer process can be represented as Yb^{3+}($^2F_{5/2}$), Er^{3+} ($^4I_{15/2}$) → Yb^{3+}($^2F_{7/2}$), Er^{3+} ($^4I_{11/2}$). A subsequent energy transfer from Yb^{3+}($^2F_{5/2}$) to excited Er^{3+}($^4I_{11/2}$) ions further promotes Er^{3+} to the $^4S_{3/2}$, $^2H_{11/2}$ excited-state manifold, from which green upconversion emission (Er^{3+}: $^4S_{3/2}$, $^2H_{11/2}$ → $^4I_{15/2}$) occurs centered at ∼540 nm.

Red upconversion (Er^{3+}: $^4F_{9/2}$ → $^4I_{15/2}$), centered at ∼660 nm, can occur either following Er^{3+}: $^4S_{3/2}$, $^2H_{11/2}$ → $^4F_{9/2}$ relaxation or via a separate feeding mechanism involving Er^{3+}($^4I_{11/2}$) → Er^{3+}($^4I_{13/2}$) relaxation followed by Yb^{3+}($^2F_{5/2}$), Er^{3+} ($^4I_{13/2}$) → Yb^{3+}($^2F_{7/2}$), Er^{3+} ($^4F_{9/2}$) energy transfer. At higher NIR pump powers, significant red upconversion can also result from Er^{3+}($^4S_{3/2}$, $^2H_{11/2}$), Er^{3+} ($^4I_{15/2}$) → Er^{3+} ($^4I_{9/2}$), Er^{3+} ($^4I_{13/2}$) cross relaxation followed by Yb^{3+}($^2F_{5/2}$), Er^{3+} ($^4I_{13/2}$) → Yb^{3+}($^2F_{7/2}$), Er^{3+} ($^4F_{9/2}$) energy transfer.[19,35] The onset of this mechanism, which is strongly dependent on Er^{3+} concentration, is manifested through an increase in the red-to-green upconversion intensity ratio.

Weak blue upconversion (Er^{3+}: $^2H_{9/2}$ → $^4I_{15/2}$) centered at ∼410 nm is also observed, resulting from energy transfer from Yb^{3+}($^2F_{5/2}$) to Er^{3+}($^4F_{9/2}$), which can be represented as Yb^{3+}($^2F_{5/2}$), Er^{3+} ($^4F_{9/2}$) → Yb^{3+}($^2F_{7/2}$), Er^{3+} ($^4G_{11/2}$).

A 45 μm × 45 μm confocal-microscope scan of 540 nm upconversion emission (λ_{ex} = 980 nm, cw) from a 240 nm thick film of ∼72 nm sized β-NaYF$_4$:3%Er,17%Yb nanocrystals in PMMA on a glass slide is shown in the upper segment of Figure 3. The scan was acquired at the Center for Nanoscale Materials at Argonne National Laboratories. The image in Figure 3 is represented in 3D mode, for which the feature height is proportional to 540 nm emission intensity (kilocounts/s, kcps). Numerous scans of other areas of the same film and similar films confirm that the Figure 3 scan is representative. The Er^{3+} upconversion emission spectra obtained from various points on the film, labeled A−D, are also shown in the lower section of Figure 3. The spectra are dominated by green ($^2H_{11/2}$,$^4S_{3/2}$→$^4I_{15/2}$) and red ($^4F_{9/2}$→$^4I_{15/2}$) emission, but blue emission ($^2H_{9/2}$→$^4I_{15/2}$) is also evident. We note that the spectral signature of upconversion is very similar at all points on the film. The average pixel
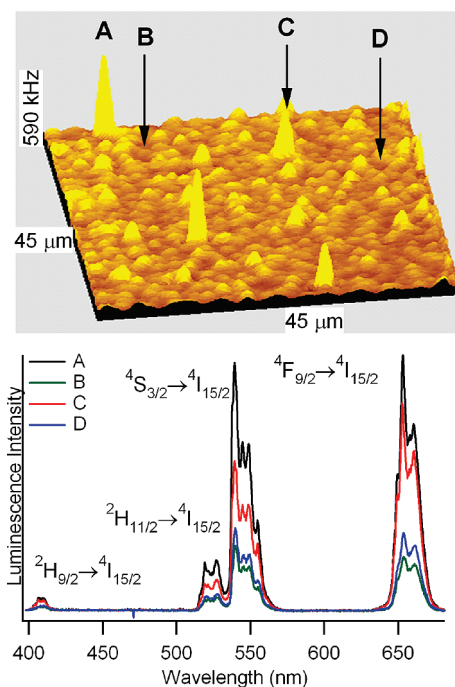

Figure 3. (Top) Confocal-microscope scan of 540 nm upconversion emission (λ_{ex} = 980 nm) from a 240 nm thick film of ∼72 nm sized β-NaYF$_4$:3%Er,17%Yb nanocrystals in PMMA on a glass slide; (bottom) upconversion emission spectra obtained from marked areas on the confocal image.

intensity in the confocal image is 31 ± 18 kcps, although there are "hot spots" for which signals are as high as 590 kcps. The confocal images of downconversion luminescence for the same films (not shown) show very similar patterns to that in Figure 3. Given the similarity of the upconversion spectra acquired from the bright regions relative to the dimmer regions, it is reasonable to attribute the inhomogeneity of upconversion intensity to occasional clustering of UC nanocrystals, and not to any fundamental differences in film composition. This clustering hypothesis is supported by TEM data, as discussed later in this section.

As demonstrated subsequently, the confocal image in Figure 3 was obtained in the high pump-power limit, in which UC intensity increases linearly with excitation power. Suyver, et al. have reported that the integrated photon flux of red and green upconversion from micrometer-sized powders of this material are nearly equal in this limit,[35] which is consistent with our own observations.

Figure 4 shows a TEM image of a film prepared identically to that in Figure 3 on a TEM grid. Based on TEM, the size of the β-NaYF$_4$:3%Er,17%Yb nanocrystals in the film is 72 ± 15 nm. For the most part, the confocal image in Figure 3 is produced by submonolayer coverage of nanocrystals within the 240 nm-thick film. As stated previously, "hot spots" in the confocal image are presumably due to occasional aggregates of nanocrystals in the film. Wide-field TEM images clearly show nanocrystal aggregation patterns within the films that are consistent with the inhomogeneity observed in the confocal image in Figure 3. A representative
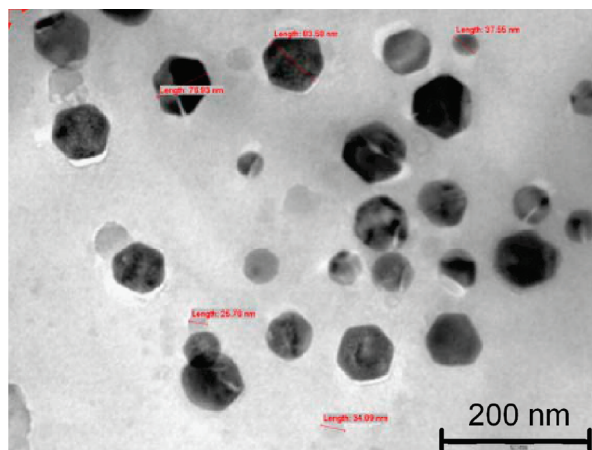
Figure 4. TEM image of thin film of NaYF$_4$:3%Er,17%Yb nanocrystals in PMMA on a TEM grid. Sample was prepared identically to that in Figure 3.
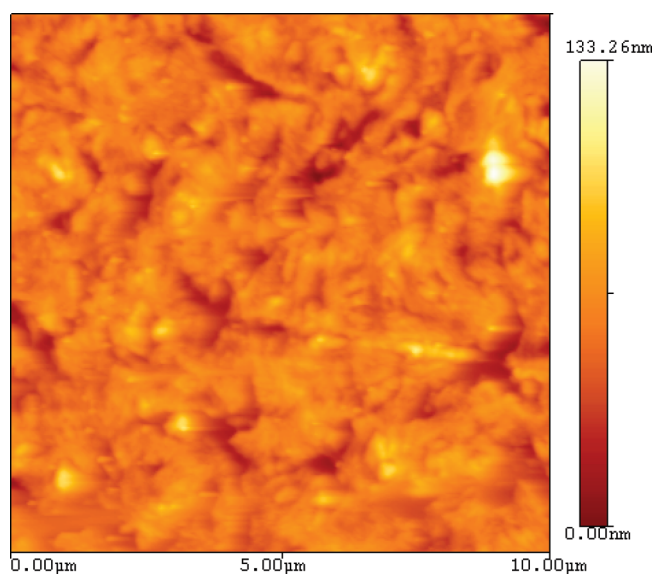
Figure 5. AFM image of sample used to obtain the confocal scan shown in Figure 3. The image shows that the majority of the NaYF$_4$:3%Er, 17%Yb nanocrystals are fully encased in the PMMA film, and only a few nanocrystals are seen to protrude from the film to any significant degree. The textured topography of the film surface is presumably due to the effect of the capped nanocrystals on the drying process during spin coating. The AFM image was obtained in noncontact mode.

wide-field TEM image is included in the Supporting Information.

AFM was used to characterize the topography and structural quality of the films. Figure 5 shows an AFM image of the surface of the same sample used to obtain the confocal image in Figure 3. AFM studies show that the film is continuous, and that the majority of the NaYF$_4$:3%Er, 17%Yb nanocrystals are fully embedded in the PMMA. Only a few nanocrystals are seen to protrude from the film to any significant degree. It is interesting to note the textured, somewhat corrugated topography of the surface. The average surface roughness determined from the scan in Figure 5 is ∼10 nm. The surface roughness of an undoped PMMA film prepared under similar conditions is only ∼0.3 nm. The increased topography of the doped film is presumably due to the
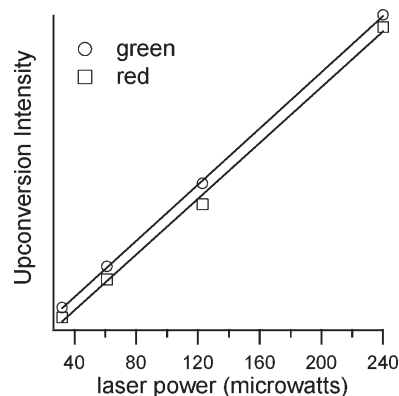

Figure 6. Pump-power dependence of green (open circles) and red (open squares) upconversion emission intensity using 980 nm cw laser excitation from 40 to 240 μW. Measurements were made on the thin film shown in Figure 3 using the confocal microscope apparatus. The intensity of the green and red upconversion was obtained by integrating the Er^{3+}: ^{4}S$_{3/2}$, ^{2}H$_{11/2}$ → ^{4}I$_{15/2}$ and Er^{3+}: ^{4}F$_{9/2}$ → ^{4}I$_{15/2}$ peaks in the upconversion spectrum, respectively.

effect of the capped nanocrystals on the drying process during spin coating.

Figure 6 shows the power dependence of both the red (Er^{3+}: ^{4}F$_{9/2}$ → ^{4}I$_{15/2}$) and green (Er^{3+}: ^{4}S$_{3/2}$, ^{2}H$_{11/2}$ → ^{4}I$_{15/2}$) upconversion emission using 980 nm cw laser-excitation powers ranging from 40 to 240 μW. Power-dependence measurements were made on the thin film shown in Figure 3 using the confocal microscope apparatus. Clearly, both red and green upconversion show linear power dependence in this region. This linear response is obtained in the so-called "high-power regime."[36] The color balance is, therefore, independent of excitation power, which is important for many display applications. We note that 40 μW was the lowest power at which stable laser operation could be maintained. Therefore, using a tightly focused excitation source, the high-power excitation regime for this sample is easily achieved. (The blue upconversion (Er^{3+}: ^{2}H$_{9/2}$ → ^{4}I$_{15/2}$) was too weak to permit accurate determination of the excitation power dependence, but its contribution to the total upconversion luminescence is too small to significantly affect color balance.) Another advantage to operating in the high-power regime is the high intrinsic luminescence quantum efficiency of β-NaYF$_4$:3%Er, 17%Yb observed under these conditions. In this limit ∼50% of absorbed NIR photons are directly involved in mechanisms leading to upconversion luminescence.[19] Mai et al. have proposed that the upconversion behavior of NaYF$_4$:Er,Yb nanocrystals approach that of the bulk material when nanocrystal size is ≥70 nm,[24] a criterion met by the nanocrystals used in this study.

Upconversion Kinetics. Figure 7 shows the time dependence of green (Er^{3+}: ^{4}S$_{3/2}$, ^{2}H$_{11/2}$ → ^{4}I$_{15/2}$) and red (Er^{3+}: ^{4}F$_{9/2}$ → ^{4}I$_{15/2}$) upconversion luminescence, respectively, following pulsed (∼6 ns) NIR excitation of the thin film. The delayed nature of the UC emission is consistent

(36) Suyver, J. F.; Aebischer, A.; García-Revilla, S.; Gerner, P.; Güdel, H. U. *Phys. Rev. B* **2005**, *71*, 125123.
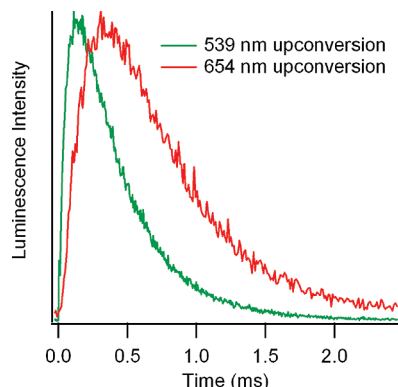
Figure 7. Time evolution of green (539 nm) and red (654 nm) upconversion luminescence, following pulsed 984 nm excitation, from a thin film of β-NaYF$_4$:3%Er,17%Yb nanocrystals in PMMA on a glass slide.

Table 1. Comparison of Upconversion Kinetics Rate Constants for β-NaYF$_4$: 3%Er,17%Yb Nanocrystals (72 nm) in Various Matrix Materials[a]

β-NaYF$_4$:3%Er, 17%Yb nanocrystal matrix	green upconversion		red upconversion	
	k_1 (s^{-1})	k_2 (s^{-1})	k_1 (s^{-1})	k_2 (s^{-1})
dry nanocrystals	2643 ± 5	18112 ± 67	2199 ± 17	5074 ± 52
hexane	2504 ± 6	15826 ± 80	2150 ± 32	4100 ± 75
chloroform	2370 ± 6	13576 ± 67	2100 ± 40	3518 ± 80
toluene	2773 ± 9	12217 ± 106	2202 ± 28	4826 ± 82
PMMA film	2720 ± 15	18691 ± 212	2035 ± 44	5462 ± 166

[a] Rate constants k_1 and k_2 were obtained by fitting the time dependence of UC emission following pulsed NIR excitation to eq 1.

with the mechanism outlined in Figure 2. Immediately following the NIR excitation pulse, only Yb^{3+} ions are excited and neither the red, Er^{3+} (^{4}F$_{9/2}$), nor the green, Er^{3+} (^{4}S$_{3/2}$, ^{2}H$_{11/2}$), emitting states are populated. UC emission intensity then builds with time as consecutive energy-transfer events from Yb^{3+}(^{2}F$_{5/2}$) feed the ^{4}S$_{3/2}$, ^{2}H$_{11/2}$ and ^{4}F$_{9/2}$ emitting levels of Er^{3+}. Finally, UC intensity diminishes as the reservoir of Yb^{3+}(^{2}F$_{5/2}$) donors becomes depleted.

The observation that red UC lags behind green UC is consistent with the feeding mechanisms of Er^{3+}:^{4}F$_{9/2}$ illustrated in Figure 2, all of which involve at least one additional intermediate state relative to the green UC mechanism. We note that the time dependence of red upconversion illustrated in Figure 7 is not consistent with Er^{3+} (^{4}F$_{9/2}$) being fed solely from the green-emitting state, Er^{3+} (^{4}S$_{3/2}$, ^{2}H$_{11/2}$). In other words, it is not possible to fit the time dependence of red upconversion assuming that Er^{3+} (^{4}F$_{9/2}$) is being directly fed by a single state exhibiting the population kinetics observed for green upconversion. This is evidence that one or more of the additional red-upconversion mechanisms discussed above, and illustrated in Figure 2, must play a significant role.

The kinetics of upconversion emission in the thin PMMA films, following pulsed NIR excitation, was compared to that observed in various other media, because the rate constants describing emission kinetics are sensitive to nonradiative relaxation pathways. Comparing the upconversion emission kinetics for β-NaYF$_4$: 3%Er,17%Yb nanocrystals in different media therefore enables an assessment of the relative quenching effect of a given host material. To the best of our knowledge, this is the first published report of the upconversion photokinetics for β-NaYF$_4$:Er,Yb.

A complete description of the photophysical kinetics leading to UC following pulsed NIR excitation requires the solution of a relatively complex set of coupled rate equations,[33,37] for which the values of many of the relevant microscopic rate constants are not known. For present purposes, however, the time dependence of green

(37) Gamelin, D. R.; Güdel, H. U. *Top. Curr. Chem.* **2001**, *214*, 1–56.

and red upconversion, $I(t)$, could be fit adequately well to the following equation

$$I(t) = A(e^{-k_1 t} - e^{-k_2 t}) \qquad (1)$$

where A is a scaling constant and k_1 and k_2 are rate constants. We emphasize that eq 1 is being used in a completely empirical manner, and that the rate constants are phenomenological. The important consideration here is that differences in nonradiative quenching efficiencies at any point along the UC mechanistic pathway will assuredly affect the fitted values of the empirical rate constants, k_1 and k_2. Therefore, a comparison of fitted k_1 and k_2 values can be used to assess the quenching effects of various matrices on UC of the nanocrystals.

Table 1 compares the k_1 and k_2 values obtained by fitting eq 1 to the time dependence of red and green upconversion following pulsed NIR excitation for (1) the dry β-NaYF$_4$:3%Er,17%Yb nanocrystals; (2) nanocrystals dispersed in hexane; (3) nanocrystals dispersed in chloroform; (4) nanocrystals dispersed in toluene; and (5) nanocrystals dispersed in 240 nm thick films of PMMA spin-coated on a glass slide. Each of the samples represented in Table 1 was prepared using nanocrystals produced from the same synthetic batch.

The values for k_1 and k_2 show only modest variation for β-NaYF$_4$:3%Er,17%Yb nanocrystals in dry-powder form, or dispersed in hexane, chloroform, toluene, and PMMA. The results in Table 1 indicate that the UC kinetics of the ~72 nm sized nanocrystals used in this study are determined largely by the relaxation processes intrinsic to the nanocrystals (including the capping ligands), and that the PMMA matrix does not significantly lower the relative intrinsic quantum efficiency of upconversion. In addition, the thickness of the PMMA film had no effect on rate constant values down to ~200 nm, below which point it was difficult to produce continuous films. We note that the k_2 values are sensitive to the power density of the laser-excitation pulse, which is affected both by the absolute laser-pulse power and the tightness of laser focus on the sample. Therefore, some of the variation in the k_2 values in Table 1 is due to small, but inevitable, differences in the excitation beam profile from sample to sample. We have minimized this effect to the greatest extent possible by acquiring all of the data in Table 1 using an identical experimental configuration within one experimental session.

Table 2. Comparison of Upconversion Kinetics Rate Constants for β-NaYF$_4$: 3%Er,17%Yb Nanocrystals in Hexane As a Function of Nanocrystal Size[a]

β-NaYF$_4$:3%Er, 17%Yb nanocrystal size (nm)	green upconversion		red upconversion	
	k_1 (s^{-1})	k_2 (s^{-1})	k_1 (s^{-1})	k_2 (s^{-1})
12 ± 3	12164 ± 47	79799 ± 611	7141 ± 104	24399 ± 545
72 ± 15	2504 ± 6	15826 ± 80	2150 ± 32	4100 ± 75
106 ± 15	1779 ± 80	12100 ± 110	1697 ± 112	2463 ± 184

[a] Rate constants k_1 and k_2 were obtained by fitting the time dependence of UC emission following pulsed NIR excitation to eq 1.

Table 2 shows a comparison of the UC rate constants for β-NaYF$_4$:3%Er,17%Yb nanocrystals dispersed in hexane as a function of nanocrystal size. (The size of nanocrystals in all samples presented to this point is 72 ± 15 nm.) We have also applied our synthetic method to make nanocrystals of size greater than 100 nm, and observe only a modest reduction in the k_1 and k_2 values. On the other hand, we have measured the UC kinetics of $\sim$14 nm sized β-NaYF$_4$:3%Er,17%Yb nanocrystals prepared using a modified method of the cothermolysis of Na(CF$_3$COO) and RE(CF$_3$COO)$_3$ precursors described by Mai, et al.[25] and observe much faster UC kinetics, indicating significant quenching from nonradiative processes. The much larger k values obtained for the smaller nanocrystals are consistent with the work of Yi, et al.,[29] who reported that the UC quantum efficiency of small (10.5 ± 0.7 nm) hexagonal-phase nanocrystals of β-NaYF$_4$:2%Er,20%Yb is 1 order of magnitude smaller compared to that of the bulk material. The data in Table 2 support the assertion of Mai, et al. that the UC properties of nanocrystals of size ≥ 70 nm approach that of the bulk material.[24] This information is of significant practical importance for device design, because one would like to use the smallest nanocrystals possible (to improve dispersibility, transparency, and applications flexibility) while maintaining high intrinsic UC efficiency relative to the bulk material. Our results indicate that 70 nm nanocrystals satisfy these criteria.

Upconversion Monoliths. Finally, the composite method can be modified, using in situ polymerization, to produce large NIR-to-visible UC monoliths of high optical quality. The incorporation of inorganic nanocrystals into polymer-based materials has been shown to be an effective strategy for producing transparent composites with new functionalities.[38] For optical applications, a main advantage to nanocomposites, as opposed to traditional composites using micrometer-sized inorganic particles, is the reduced Rayleigh scatter from nanoscale particles. Small particle size also increases the homogeneity of the functional material in the composite. Figure 8 shows a photograph of UC from a cylindrical monolith of PMMA doped with 72 nm β-NaYF$_4$: 3%Er,17%Yb nanocrystals in a darkened room and under full fluorescent room lighting. Efficient NIR-to-visible UC monoliths, such as shown in Figure 8 are of interest for many applications, including 3D displays. Downing, et al.
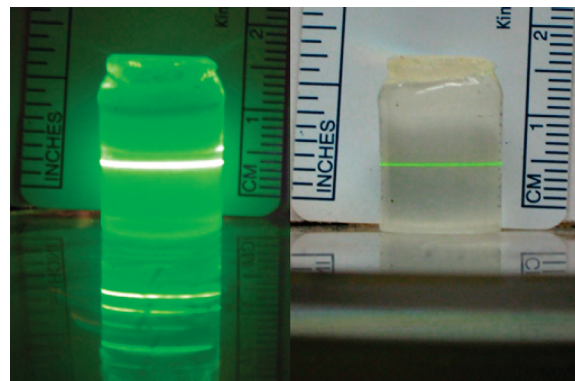
Figure 8. Cylindrical monolith of β-NaYF$_4$:3%Er,17%Yb nanocrystals in PMMA excited with a 980 nm diode laser ($\sim$200 mW) in a darkened room (left) and under full fluorescent room lighting (right).

have successfully demonstrated prototypes of both monochrome and multicolor 3D displays based on the UC of lanthanide-doped fluoride glasses (such as ZBLAN) using NIR diode lasers to "draw" the image.[8] Subsequently, the advantages of activating 3D displays with UC nano crystal have been recognized. Liu et al. have suggested that colloidal dispersions of lanthanide-ion-doped NaYF$_4$ nanocrystals in various solvents can be used as a matrix for NIR-pumped 3D displays.[9] In this case, however, the stability of the matrix is limited by the stability of the dispersion. Long-term stability of the dispersions will probably require the use of vitreous matrices for the nanocrystals, as applied in the composite approach described herein.

Conclusions

This study characterizes highly luminescent upconversion thin films and monoliths that can be produced without high-temperature processing. For the UC thin films, it has been demonstrated that the high-power pump regime, for which UC intensity varies linearly with NIR pump power, and for which color balance is pump-power independent, can easily be achieved by focusing a low-power (< 40 μW) NIR pump source. Also, it should be possible to use this method to produce either red, green or blue emitting films by changing the dopants and /or morphology of the NaYF$_4$ nanocrystals.[1,24,34,35,39] Although here we have concentrated mainly on the characterization of ultrathin films, the method can adapted to produce films of virtually any thickness. We are currently developing methods for controlling the level of nanocrystal clustering in the films, and characterizing how clustering varies with film thickness. We are also investigating methodologies for producing upconverting inks for use with Direct Write technologies. The nanocrystal-composite approach to UC material design shows great promise and flexibility in terms of creating phosphor materials to suit a wide range of applications.

(38) Althues, H.; Henle, J.; Kaskel, S. *Chem. Soc. Rev.* **2007**, *36*, 1454–1465.

(39) Wang, F.; Liu, X. *J. Am. Chem. Soc.* **2008**, *130*, 5642–5643.

Article

Chem. Mater., Vol. 21, No. 14, 2009 3413

Supporting Information Available: Photographs of UC nanocrystal dispersion in chloroform, wide-field TEM image showing clustering patterns of UC nanocrystals in PMMA film, TEM images of 106 nm nanocrystals used to obtain data in Table 2, fits of UC kinetics to eq 1 (PDF). This material is available free of charge via the Internet at http://pubs.acs.org.